International Journal of Solids and Structures 47 (2010) 374–382

Contents lists available at ScienceDirect

International Journal of Solids and Structures

journal homepage: www.elsevier.com/locate/ijsolstr

Measurement method of complex viscoelastic material properties

Andrey V. Boiko [a], Victor M. Kulik [b], Basel M. Seoudi [c], H.H. Chun [d], Inwon Lee [d,*]

[a] Institute of Theoretical and Applied Mechanics, Russian Academy of Sciences, Novosibirsk 630090, Russia
[b] Institute of Thermophysics, Russian Academy of Sciences, Novosibirsk 630058, Russia
[c] Department of Marine Engineering Technology, Arab Academy for Science, Technology and Maritime Transport, Alexandria, P.O. Box 1029, Egypt
[d] Advanced Ship Engineering Research Center (ASERC), Pusan National University, Busan 609-735, Republic of Korea

ARTICLE INFO

Article history:
Received 7 August 2008
Received in revised form 4 May 2009
Available online 1 October 2009

Keywords:
Measurement technique
Shear modulus
Modulus of elasticity
Poisson's ratio
Shear and elastic vibrations

ABSTRACT

A measurement technique of viscoelastic properties of polymers is proposed to investigate complex Poisson's ratio as a function of frequency. The forced vibration responses for the samples under normal and shear deformation are measured with varying load masses. To obtain modulus of elasticity and shear modulus, the present method requires only knowledge of the load mass, geometrical characteristics of a sample, as well as both the amplitude ratio and phase lag of the forcing and response oscillations. The measured data were used to obtain the viscoelastic properties of the material based on a 2D numerical deformation model of the sample. The 2D model enabled us to exclude data correction by the empirical form factor used in 1D model. Standard composition (90% PDMS polymer + 10% catalyst) of silicone RTV rubber (Silastic® S2) were used for preparing three samples for axial stress deformation and three samples for shear deformation. Comprehensive measurements of modulus of elasticity, shear modulus, loss factor, and both real and imaginary parts of Poisson's ratio were determined for frequencies from 50 to 320 Hz in the linear deformation regime (at relative deformations 10^{-6} to 10^{-4}) at temperature 25 °C. In order to improve measurement accuracy, an extrapolation of the obtained results to zero load mass was suggested. For this purpose measurements with several masses need to be done. An empirical requirement for the sample height-to-radius ratio to be more than 4 was found for stress measurements. Different combinations of the samples with different sizes for the shear and stress measurements exhibited similar results. The proposed method allows one to measure imaginary part of the Poisson's ratio, which appeared to be about 0.04–0.06 for the material of the present study.

1. Introduction

After influential studies of Cauchy, Green, Stokes and other founders of material strength theory it is now commonly accepted that elastic properties of an isotropic material are characterized by only two parameters (Timoshenko, 1953). Accordingly, any deformation field can be expanded into two elementary components of volume-conservative shear deformations and volume-nonconservative elastic deformations (Landau and Lifschitz, 1986).

The relation between the deformation and the applied shear stress can be expressed through the shear modulus G. Similarly, the deformation due to uniform compression is associated with the bulk modulus K, which is one of the thermodynamic parameters of material. This is because $K = -\frac{V}{(\partial V/\partial P)_T}$ is associated with the isothermal compressibility $\left(\frac{\partial V}{\partial P}\right)_T$. Besides these fundamental material properties, the modulus of elasticity E and the Poisson's ratio v are used frequently in practice. The modulus of elasticity E characterizes the relation between an applied axial load and one-dimensional deformation of a thin long rod. In the simplest case the following Hooke's law is hold:

$$E = \frac{F}{S}\frac{\Delta\ell}{\ell},$$

where F is the applied force and S is the cross section of the rod. ℓ and $\Delta\ell$ are the rod length and the elongation, respectively. Poisson's ratio, which is the ratio between the lateral contraction to the axial elongation, is given as (Landau and Lifschitz, 1986)

$$v = \frac{1}{2}\frac{3K - 2G}{3K + G}.$$

Since K and G are always positive, the Poisson's ratio varies for different materials from -1 (with $K = 0$) to 0.5 (with $G = 0$). Poisson's ratio $v \approx 0.5$ corresponds to small shear modulus G compared with the bulk modulus K. The parameters are related to each other as

$$K = \frac{E}{2(1-2v)}, \quad G = \frac{E}{2(1+v)}.$$

Hence, it is sufficient to know only two among the four parameters to calculate a three-dimensional linear deformation. Also, the Lame coefficients, which are combinations of K and G, are used

* Corresponding author. Tel.: +82 51 510 2764; fax: +82 51 581 3718.
E-mail address: inwon@pusan.ac.kr (I. Lee).

0020-7683/$ - see front matter © 2009 Elsevier Ltd. All rights reserved.
doi:10.1016/j.ijsolstr.2009.09.037

sometimes. Thus, to determine the elastic properties of a material it is essential to perform two experiments with two different kinds of the deformation. In the ideal case they are the pure shear deformations and the normal deformations. The latter, however, is replaced frequently by bending, where the resulting deformation is a superposition of the shear deformations and the normal deformations.

Under the action of dynamic loading, the deformation of viscoelastic material from its equilibrium position can occur with a certain delay due to viscous friction inside the material. Under harmonic forcing, this delay manifests itself by a phase shift between the applied load and the deformation. The shift is proportional to the viscous losses in the material. Besides, the modulus of elasticity and the shear modulus become frequency dependent complex functions

$$E^* = Re(E^*) + iIm(E^*) = E(1 + i\mu^E)$$
$$G^* = Re(G^*) + iIm(G^*) = G(1 + i\mu^G),$$

where μ^E and μ^G are loss tangents for stress and shear deformations. If the Poisson's ratio at dynamic deformations is real, then $\mu^E = \mu^G = \mu$. Nonzero imaginary part of the Poisson's ratio means that there is a phase delay or lead of a transverse strain with respect to the axial strain under dynamic deformation, in which case μ^E and μ^G can be different.

Ferry (1961) and Riande et al. (2000) summarized a number of studies devoted to the description of these dynamical properties of materials. Recently there appeared theoretical substantiation of possibility of complex-number frequency dependent Poisson's ratios (Tschoegl et al., 2002; Lakes and Wineman, 2006). Literature survey reveals that the attempts to study Poisson's ratio behavior as a function of frequency from direct experiments are as follows.

Kästner and Pohl (1963) found a decrease of the real part of ν from 0.5 at $f = 5 \times 10^{-4}$ to 0.4 at $f = 0.1$ Hz for a polymethylmethacrylate (PMMA) sample. Imaginary part of ν appeared to be small. Koppelmann (1959) measured E and G of PMMA for frequencies $f = 10^{-5}$ to 10^{-1} Hz at temperatures from 20 °C to 100 °C. It was found that the Poisson's ratio depends on neither frequency nor temperature. Giovagnoni (1994) measured axial and lateral deformations in frequency range from 80 to 720 Hz for a series of samples in glassy state. The Poisson's ratio appeared to be independent of frequency. Willis et al. (2001) determined E and G of a polyurethane using laser vibrometer and 2D model of sample deformation. Poisson's ratio was between 0.4 and 0.5 on the frequency range from 200 to 2000 Hz.

Besides, indirect measurements of the Poisson's ratio by means of deformation measurements at different temperatures by applying the temperature–frequency analogy of Williams–Landel–Ferry are also quite sporadic and controversial (see, e.g., Crowson and Arridge, 1979; Hausler et al., 1987 for review). Direct experimental determination of the Poisson's ratio requires high accuracy of the measurements and must follow the standard protocol, which includes:

- samples of the same material,
- measurements at the same temperatures and pressures,
- synchronism of the measurements.

Furthermore, the polymer samples should be prepared from a homogeneous and isotropic material and its deformation should be small to provide its linearity. Hence, the number of parameters required to describe dynamic elastic deformation of a homogeneous material is essentially doubled compared to the static case. However, the question whether the Poisson's ratio becomes really complex (and if so, than at which conditions) and frequency dependent function is still open and requires further clarification.

The absence of systematic measurements of the Poisson's ratio for viscoelastic polymers in different temperature and frequency regions can be explained partly by both the lack of reliable experimental techniques and the absence of standard facilities. For frequencies higher than 100 Hz, there exist several methods of measurement of modulus of elasticity (or shear modulus) and loss factor. They are described in review of Ferry (1961) and recent example of Clifton et al. (2006). The method of measurements of the modulus of elasticity and the loss factor used in Kulik and Semenov (1986), Kulik et al. (2008) covers the frequency range from 10 to 10 kHz at relative values of deformation of orders 10^{-4}% to 5%. The method is essentially easy-to-operate and reliable requiring no mechanical tuning and adjustment, the measurement results being independent from the vibrator characteristics. In the present study, this technique is extended allowing one to measure additionally the dynamic shear modulus. Using raw measurement results of both axial and shear deformations for the samples prepared simultaneously from the same mixture, three-dimensional deformations of the samples were calculated and the complex values of E, G and ν have been estimated.

2. Mathematical model

2.1. Governing equations

Fig. 1 describes the samples under considerations in this study. The cylindrical sample with radius R in Fig. 1(a) undergoes axial deformations while the annular sample in Fig. 1(b) is associated with shear deformations. The inner and outer radius of the annular sample are R_0 and R_1, respectively. Both samples have the same mass m and height H. The samples consist of the viscoelastic material with the modulus of elasticity E, loss factor μ and (assumed complex-valued) Poisson's ratio ν. The samples are bonded to the oscillating table on one side and loaded with a mass M on the other side. The table oscillates harmonically with amplitude A_0 and frequency ω. The load mass M attached on the other side of the sample exhibits the same frequency of oscillation with the amplitude ZA_0 and the phase lag θ.

Displacement of any point inside the samples in the laboratory cylindrical coordinate is described by two components

$$\vec{\xi} = \zeta(r,z)\hat{e}_z + \eta(r,z)\hat{e}_r,$$

where $\eta(r,z)$ is the radial displacement and $\zeta(r,z)$ is the axial displacement. The stress–strain relations are the form

$$\sigma_{rr} = E(1+i\mu)\left[\frac{\nu}{(1-2\nu)(1+\nu)}\left(\frac{\partial\eta}{\partial r}+\frac{\eta}{r}+\frac{\partial\zeta}{\partial z}\right)+\frac{1}{1+\nu}\frac{\partial\eta}{\partial r}\right]$$
$$\sigma_{zz} = E(1+i\mu)\left[\frac{\nu}{(1-2\nu)(1+\nu)}\left(\frac{\partial\eta}{\partial r}+\frac{\eta}{r}+\frac{\partial\zeta}{\partial z}\right)+\frac{1}{1+\nu}\frac{\partial\zeta}{\partial z}\right]$$
$$\sigma_{zr} = \frac{E(1+i\mu)\nu}{2(1+\nu)}\left(\frac{\partial\eta}{\partial z}+\frac{\partial\zeta}{\partial r}\right)$$

The governing equation for two-dimensional elastic wave in isotropic medium (Landau and Lifschitz, 1986) takes the form

$$\frac{\partial^2\vec{\xi}}{\partial t^2} = C_t^2\Delta\vec{\xi} + \left(C_\ell^2 - C_t^2\right)\nabla(\nabla\cdot\vec{\xi}), \tag{1}$$

where $C_t^2 = \frac{E(1+i\mu)}{2\rho(1+\nu)}$, $C_\ell^2 = \frac{E(1+i\mu)(1-\nu)}{\rho(1+\nu)(1-2\nu)}$, $\rho = \frac{m}{\pi R^2 H}$.

If torsional oscillations are excluded from the considerations and harmonic loading is assumed, then the Navier equation in Eq. (1) can be written explicitly as

$$\begin{aligned} &C_\ell^2\left(r\tfrac{\partial\eta}{\partial r}-\eta+r^2\tfrac{\partial^2\eta}{\partial r^2}+r^2\tfrac{\partial^2\zeta}{\partial r\partial z}\right)+C_t^2 r^2\left(\tfrac{\partial^2\eta}{\partial z^2}-\tfrac{\partial^2\zeta}{\partial r\partial z}\right)+r^2\omega^2\eta=0,\\ &C_\ell^2\left(r\tfrac{\partial^2\eta}{\partial r\partial z}+\tfrac{\partial\eta}{\partial z}+r\tfrac{\partial^2\zeta}{\partial z^2}\right)+C_t^2\left(\tfrac{\partial\zeta}{\partial r}-\tfrac{\partial\eta}{\partial z}+r\tfrac{\partial^2\zeta}{\partial r^2}-r\tfrac{\partial^2\eta}{\partial r\partial z}\right)+r\omega^2\zeta=0. \end{aligned} \tag{2}$$

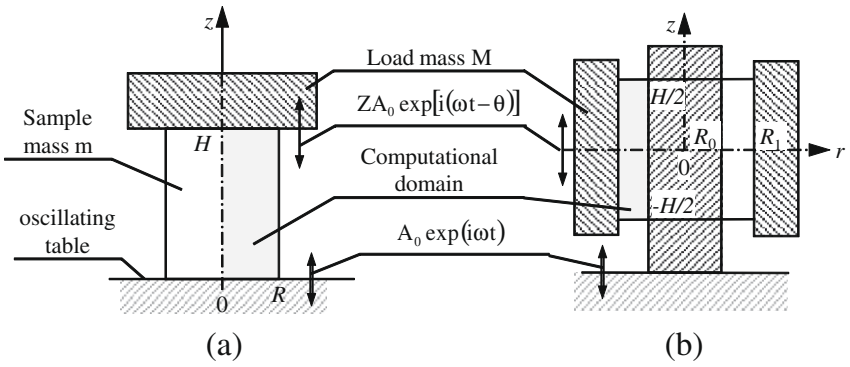

Fig. 1. Schematic diagram of samples; (a) cylindrical sample under axial deformation and (b) annular sample under shear deformation.

One can assume in the beginning that Poisson's ratio is known and the unknown values are only E and μ. The procedure consists in repeated determination of E_1, E_2 and μ_1, μ_2 for a pair of the samples with different load masses and at different assumed values of Poisson's ratios as described in the rest of this section. This allows finding ν in further postprocessing as discussed in more detail in Section 3.3 and illustrated in Fig. 7.

2.2. Boundary conditions for cylindrical sample

The boundary conditions in cylindrical coordinate system can be categorized as follows (see Fig. 1(a)):

(a) Absence of radial displacements at bonded surfaces

$$\eta = 0 \text{ at } z = 0, \tag{3}$$
$$\eta = 0 \text{ at } z = H, \tag{4}$$

(b) Axial harmonic displacements at the lower and upper surfaces

$$\zeta = A_0 e^{i\omega t} \text{ at } z = 0, \tag{5}$$
$$\zeta = ZA_0 e^{i(\omega t-\theta)} \text{ at } z = H, \tag{6}$$

(c) Absence of stresses at the side surface (at $r = R$)

$$\sigma_{rz} = 0 \to \frac{\partial \eta}{\partial z} + \frac{\partial \zeta}{\partial r} = 0, \tag{7}$$
$$\sigma_{rr} = 0 \to (1-\nu)\frac{\partial \eta}{\partial r} + \nu\left(\frac{\partial \zeta}{\partial z} + \frac{\eta}{r}\right) = 0, \tag{8}$$

This condition to be fulfilled on the mobile sidewall of a sample greatly complicates the solution procedure. For simplicity and possibility of solving these equations on personal computer, it is suggested that the boundary conditions of Eqs. (7) and (8) be applied at $r = R$. In Section 3.3 the results of this simplification are discussed and the realization method of correct boundary condition on the sample sidewall is suggested.

To obtain E and μ, after normalization of the displacements η and ζ by oscillation amplitude A_0 in Eqs. (2)–(8), only Z and θ need to be measured during tests. Then, the procedure to obtain E and μ is to solve an inverse problem defined by Eqs. (2)–(8). Toward this end, measured data of the oscillation magnitude ratio $Z$and the phase delay θ are utilized. Unique solution is obtained with the help of the following compatibility condition

$$M\frac{\partial^2 \zeta}{\partial t^2} = -2\pi \int_0^R \sigma_{zz}(H, r) r dr, \tag{9}$$

which equates internal stress at the upper edge with the pressure developed by the movement of the finite load mass M. After combining Eq. (6) and $\sigma_{zz} = \frac{E(1+i\mu)(1-\nu)}{(1+\nu)(1-2\nu)}\frac{\partial \zeta}{\partial z}$ in Eq. (9), we have finally

$$MZ\omega^2 e^{i(\omega t-\theta)} = 2\pi \frac{E(1+i\mu)(1-\nu)}{(1+\nu)(1-2\nu)} \int_0^R \frac{\partial \zeta}{\partial z}(H, r) r dr. \tag{10}$$

2.3. Boundary conditions for annular sample

The boundary conditions in this case can be categorized as follows (see Fig. 1(b)):

(a) Absence of radial displacements at bonded surfaces

$$\eta = 0 \text{ at } r = R_0, \tag{11}$$
$$\eta = 0 \text{ at } r = R_1, \tag{12}$$

(b) Axial harmonic displacements at the inner and outer surfaces

$$\zeta = A_0 e^{i\omega t} \text{ at } r = R_0, \tag{13}$$
$$\zeta = ZA_0 e^{i(\omega t-\theta)} \text{ at } r = R_1, \tag{14}$$

(c) Absence of stresses at the upper and lower surfaces (at $z = \pm H/2$)

$$\sigma_{rz} = 0 \to \frac{\partial \eta}{\partial z} + \frac{\partial \zeta}{\partial r} = 0, \tag{15}$$
$$\sigma_{zz} = 0 \to (1-\nu)\frac{\partial \zeta}{\partial z} + \nu\left(\frac{\partial \eta}{\partial r} + \frac{\eta}{r}\right) = 0, \tag{16}$$

The compatibility condition to obtain unique solution in this case becomes

$$M\frac{\partial^2 \zeta}{\partial t^2}(z, R_1) = -4\pi R_1 \int_0^{H/2} \sigma_{rr}(z, R_1) dz$$

After combining Eqs. (12), (14) and $\sigma_{rr} = \frac{E(1+i\mu)(1-\nu)}{(1+\nu)(1-2\nu)}\frac{\partial \eta}{\partial r}$, we have finally

$$MZ\omega^2 e^{i(\omega t-\theta)} = \frac{4\pi R_1 E(1+i\mu)(1-\nu)}{(1+\nu)(1-2\nu)} \int_0^{H/2} \frac{\partial \eta}{\partial r}(z, R_1) dz. \tag{17}$$

2.4. Solution procedure

To solve the governing equations numerically, a pseudospectral approximation of the wave equations with $N_z \times N_r$ mesh points was employed (Canuto et al., 1988). A grid was set up based on Chebyshev Gauss–Lobatto knots independently in z and r, producing tensor product grid. Let the rows and columns of the $(N+1) \times (N+1)$ Chebyshev spectral differentiation matrix D_N be indexed from 0 to N. The entries of this matrix are given by the following rules (Canuto et al., 1988; Trefethen, 1990)

$$(D_N)_{00} = \frac{2N^2+1}{6}, (D_N)_{NN} = -(D_N)_{00},$$
$$(D_N)_{jj} = \frac{-x_j}{2(1-x_j^2)}, j = 1, \ldots N-1,$$
$$(D_N)_{ij} = \frac{c_i}{c_j}\frac{(-1)^{i+j}}{x_i - x_j}, i \neq j, i,j = 1, \ldots N-1, \quad (18)$$

where $x_k = \cos(k\pi/N)$, $k = 0,1,\ldots,N$ and

$$c_i = \begin{cases} 2 & i = 0 \text{ or } N \\ 1 & \text{otherwise} \end{cases}. \quad (19)$$

Due to the incompatibility of the boundary conditions in the corner points at $r = R$, $z = 0$, and $r = R$, $z = H$, where the first derivative of the deformations $\partial\zeta/\partial z$and $\partial\zeta/\partial r$ may become discontinuous, the accuracy of the calculation of the integrals in Eq. (9) is relatively low (Grinchenko and Meleshko, 1981). However, the corner singularities in these cases are quite weak and a reduction of the error to an admissible value in using relatively small matrix sizes can be achieved, e.g., by an appropriate coordinate transformation, which condense the knots at the corners (Tang and Trummer, 1996). Toward this end, the following coordinate transformation was employed:

$$y = \frac{\arctan(\alpha x)}{\arctan(\alpha)}, \quad (20)$$

which mapped the polynomial domain $[-1;1] \times [-1;1]$ onto itself. Here, the scaling factor $\alpha$is nondimensional. The knots concentrate at the corners and become sparser in the bulk of the sample with increasing scaling factor α. However, when the number of knots is too limited in the bulk of the sample, the form of deformation cannot be resolved anyway, if N_z and N_r are fixed small. In the numerical tests described in the next section $\alpha = 2$ was used. This value was chosen on the trial basis to produce an "optimal" knot distribution, which is to minimize values of N_z and $N_r$for production of the results accurate enough for our purpose in the whole frequency range under study and, hence, to accelerate the calculations. It was found that as the number of knots in each direction is enlarged from 12 to 20, the approximated values of E and μ varied less than 1% in the region of interest.

Then, a linear coordinate transformation mapped the problem from the polynomial domain $[-1;1] \times [-1;1]$ to the domain $[0;H] \times [0;R]$. Specifically, the mesh $(r_i, z_j), r_i = R\cos(\frac{i\pi}{N_r}),\ z_j = \frac{H}{2}[\cos(\frac{j\pi}{N_z}) + 1],\ i = 0, \ldots, N_r/2 (N_r \text{ is even}), j = 0, \ldots, N_r$ is considered.

Let us represent the functions of displacements $\eta(r_i,z_j)$ and $\zeta(r_i,z_j)$ in the mesh points by the matrices $(\eta)_{i,j}$ and $(\zeta)_{i,j}$ and denote the first discrete derivative operators in r and $z$as $\overline{D}_r = D_{N_r}/R$ and $\overline{D}_z = 2D_{N_z}/H$, respectively. Due to the axial symmetry of the problem under consideration, we are interested only in the solution at $r \in [0;R]$, in which case the matrix $\overline{D}_r$can be reduced to the matrices $\overline{\overline{D}}_r$ for the even function $\zeta(r_i,z_j)$ and $\widetilde{\overline{D}}_r$ for the odd function $\eta(r_i,z_j)$, of which elements are given as

$$(\overline{\overline{D}}_r)_{ij} = (\overline{D}_r)_{ij} + (\overline{D}_r)_{ik},\ i,j = 0 \ldots (N+1)/2, k = N+1-j$$
$$(\widetilde{\overline{D}}_r)_{ij} = (\overline{D}_r)_{ij} - (\overline{D}_r)_{ik},\ i,j = 0 \ldots (N+1)/2, k = N+1-j. \quad (21)$$

If we reassemble the matrices η and ζ into the column vectors built by the columns of η and ζ written one by one (that is we represent them in the lexicographic order), the directional derivative matrices may be expressed as tensorial (Kroneker) products and become (Trefethen, 1990)

$$\overline{D}_r = \overline{\overline{D}}_r \otimes I_z, \quad \widetilde{D}_r = \widetilde{\overline{D}}_r \otimes I_z, \quad D_z = I_r \otimes \overline{D}_z,$$
$$\overline{D}_{rr} = \overline{\overline{D}}_r^2 \otimes I_z, \quad \widetilde{D}_{rr} = \widetilde{\overline{D}}_r^2 \otimes I_z, \quad D_{zz} = I_r \otimes \overline{D}_z^2,$$
$$\overline{D}_{rz} = \overline{\overline{D}}_r \otimes \overline{D}_z, \quad \widetilde{D}_{rz} = \widetilde{\overline{D}}_r \otimes \overline{D}_z, \quad (22)$$

where I_z and I_r are the unit $(N_z + 1)$ and $(N_r + 1)$ matrices, respectively. Then, the original system of equations is approximated by the following matrix equation

$$\begin{bmatrix} C_\ell^2(r^2\widetilde{D}_{rr} + r\widetilde{D}_r - I_r \otimes I_z) + C_t^2 r^2 D_{zz} + r^2\omega^2 & \left(C_\ell^2 - C_t^2\right)r^2\overline{D}_{rz} \\ \left(C_\ell^2 - C_t^2\right)(r\widetilde{D}_{rz} + D_z) & C_t^2(r\overline{D}_{rr} + \overline{D}_r) + C_\ell^2 r D_{zz} + r\omega^2 \end{bmatrix} \begin{pmatrix} \eta \\ \zeta \end{pmatrix} = 0. \quad (23)$$

Boundary conditions were applied explicitly by changing the corresponding rows in the left and right-hand sides of the equations (Trefethen, 1990) to make inhomogeneous problems, which are then easily solved by the left matrix division for every frequency point and every value of r. Final approximations of E and μ were obtained by Gauss–Newton iterations of the obtained solutions to satisfy the compatibility condition, Eq. (9). The calculations were performed in MATLAB.

3. Results and discussion

3.1. Material and sample preparation

Silicone RTV rubber Silastic® S2 (manufactured by Dow Corning) was used as a test material. This material is an addition-cure type elastomer and is widely used for mold-making purpose. It is one of the simplest silicon compounds (polydimethylsiloxane $[-O-Si(CH_3)_2-]_n$), which is a white fluid with viscosity 90 Poise in the original state. The standard composition is 90:10 mixture of polymer and catalyst.

Before mixing with the catalyst, the polymer was put in a depressurized chamber for several hours to remove air bubbles inside. With the catalyst being added, the mixture is polymerized at a room temperature and pressure. Typical polymerization time is about 2 h, which is long enough for injection molding to form samples of desired shape. Photos of the cylindrical and annular samples are shown in Fig. 2. Two different pairs of samples (cylindrical + annular) are presented in Fig. 3. After preparation of the samples, their masses and linear dimensions are thoroughly measured. Table 1 provides the sizes and the masses of the samples. In bonding the cylindrical samples to both the vibration table and the load mass all contact metal parts were degreased and activated by a high-tack solvent-based cold-drying primer P-11 to improve the adhesion; then the original polymer mixture was used for the bonding. The thickness of the bonding layer was negligible.

3.2. Measurement setup

The detailed description of the measurement setup can be found in Kulik et al. (2008). Fig. 4 presents the schematic diagram of the measurement setup. A miniature accelerometers (Brüel & Kjær Type 4518-001) were mounted onto the load mass and the base plate. Both accelerometers have virtually flat frequency response up to 20 kHz. The small mass (1.65 g) of the miniature load accelerometer enabled measurements with large mass ratios M/m.

The accelerometers were connected to a Brüel & Kjær NEXUS® amplifier Type 2963, in which the amplifier gains for both accelerometers were adjusted to provide equal voltage outputs for the same vibration excitations. A calibration test (shown in Fig. 5) with both accelerometers mounted on a rigid plate indicated that the magnitude and phase difference between two accelerometers were less than 0.6% and 1° over frequencies of $10 \sim 650$ Hz, respectively. In order to improve accuracy, two sensors Brüel & Kjær Type 4518-001 produced in the same lot (with neighboring Serial Nos. 50887 and 50889) were used. The residual tiny differences in their sensitivity (mainly phase shift) were compensated by a specially performed calibration.

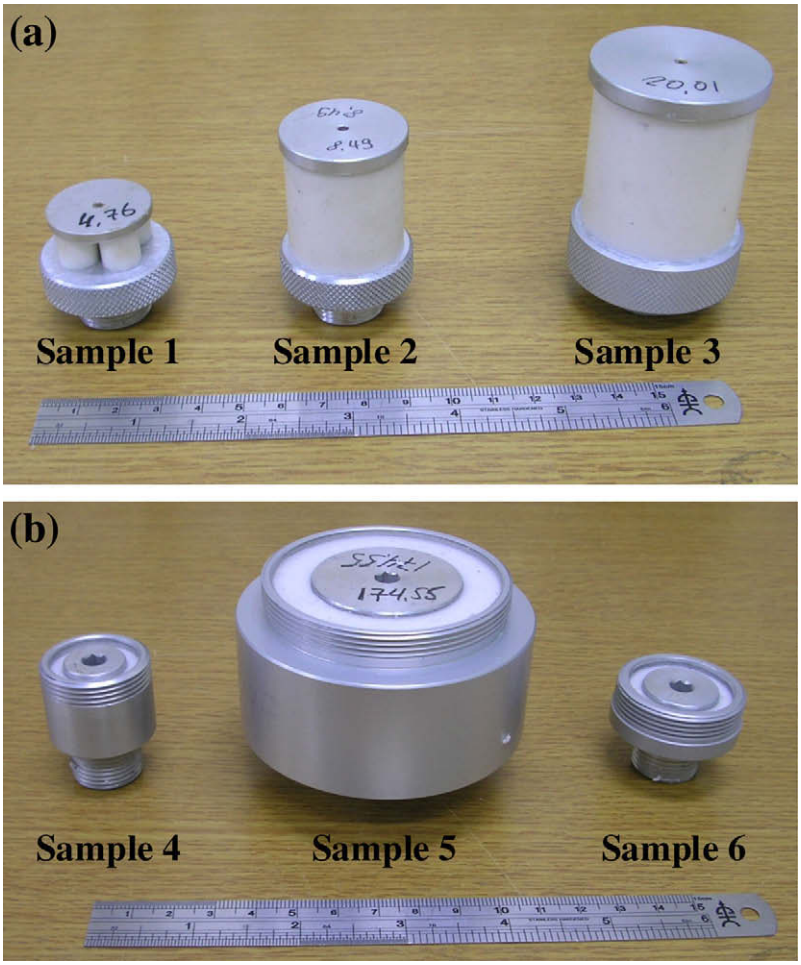

Fig. 2. Photos of the specimens; (a) cylindrical specimens and (b) annular specimens.

This calibration was made several times during experiment – before, in the middle of and after the experiment. These results showed that sensitivity of the channels remained stable. Nevertheless, we made correction of sensitivity of reference accelerometer after each calibration. Therefore, the relative vibration magnitude Z and the phase difference θ can be calculated directly from the voltage signals from each channel of the vibration amplifier.

With the help of connector block BNC-2120 and analog-to-digital converter (National Instrument PCI-6023E), the signals were digitized and logged to computer memory and to a hard disk. Each time series consisted of 100,000 instant measurements obtained with 50 kHz sampling frequency. Specially developed program controlled fully automatically the data sampling and processing, performing in particular

- Digitizing of sensor signals,
- Signal filtration to get rid of noise,
- Determination of the signal magnitude ratio Z and the phase delay θ,
- Frequency polling by a selected algorithm (with predetermined limits and the number of frequencies as well as a law of their variation),
- Maintenance of constant level of the reference signal (by either acceleration or displacement).

The measurements of the stress and shear deformation were carried out at the same frequencies to exclude the interpolation. The fixed frequencies given by formula $f = 20{\cdot}2^{n/6}$, where n changes from 0 to 30 correspond to 1/6 octave frequency spectrum. On performing two series (shear and stress) of the tests, a set of the data $\{f, Z, \theta\}$ for different load masses is obtained. The measurements were carried out at constant temperatures 25 °C. For this purpose the vibrator with the samples and sensors was placed in a temperature controlled chamber. When a new load mass is installed, the settling time of at least half an hour was provided before measurement for the temperature stabilization.

Fig. 6 demonstrates long-term aging characteristics of samples at two different frequencies. As seen, the viscoelastic properties exhibits relatively fast changes during the first 40 days and consequent very slow changes. Therefore, all measurements were carried out 2 month after preparing of the samples during 1 weak. It allowed us to avoid the ageing problem.

In order to ensure linear deformation regime, the excitation level was kept as small as possible, giving rise to the resulting deformation level in the range of 10^{-6} to 10^{-4}. It was made to avoid the nonlinear deformation and stave off heating of a sample over an internal friction.

3.3. Results

It is notable that in solving governing equations for the cases under consideration one has to fix the Poisson's ratio in advance. The calculated values E and $2G(1 + \nu)$ as functions of the Poisson's ratio in the range from 0.22 to 0.495 are plotted in Fig. 5(a) at $f = 107$ Hz. It is seen that the curves corresponding to the shear and stress measurements intersect each other in a quite narrow

Fig. 3. Photos of the various pairs of specimens.

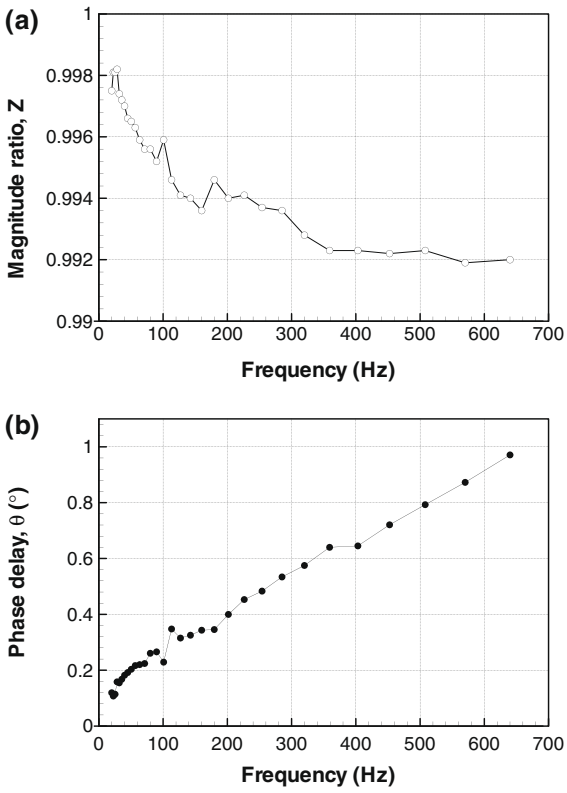

Fig. 5. Result of calibration test; (a) magnitude ratio Z and (b) phase delay θ.

Table 1
Parameters of specimens.

No.	Number of elements	Element shape	Height (mm)	Outer diameter (mm)	Inner diameter (mm)	Specimen mass (g)
1	4	Cylinder	10.05	10.0		3.58
2	1	Cylinder	30.0	30.0		23.64
3	1	Cylinder	40.0	40.0		56.0
4	1	Hollow cylinder	16.95	24.0	17.0	4.37
5	1	Hollow cylinder	40.0	60.0	40.0	71.08
6	1	Hollow cylinder	7.97	30.0	22.0	7.20

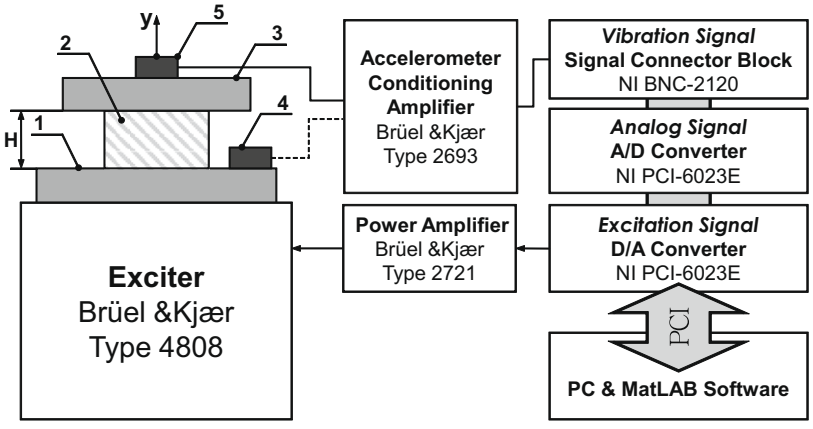

1 —Base Plate; 2 —Sample; 3 —Load Mass (M);
4 —Reference Accelerometer; 5 —Load Accelerometer

Fig. 4. Schematic diagram of measurement setup.

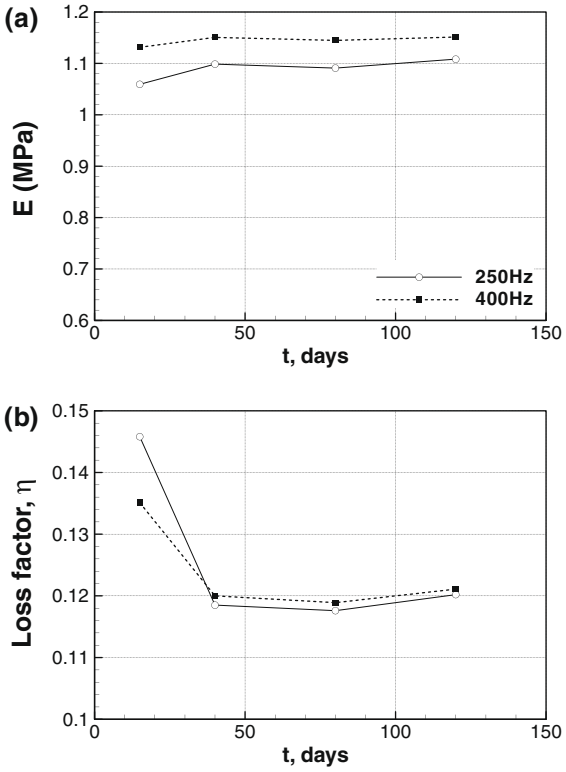

Fig. 6. Ageing of specimens at assumed Poisson's ratio ν= 0.48; (a) modulus of elasticity E and (b) loss factor μ.

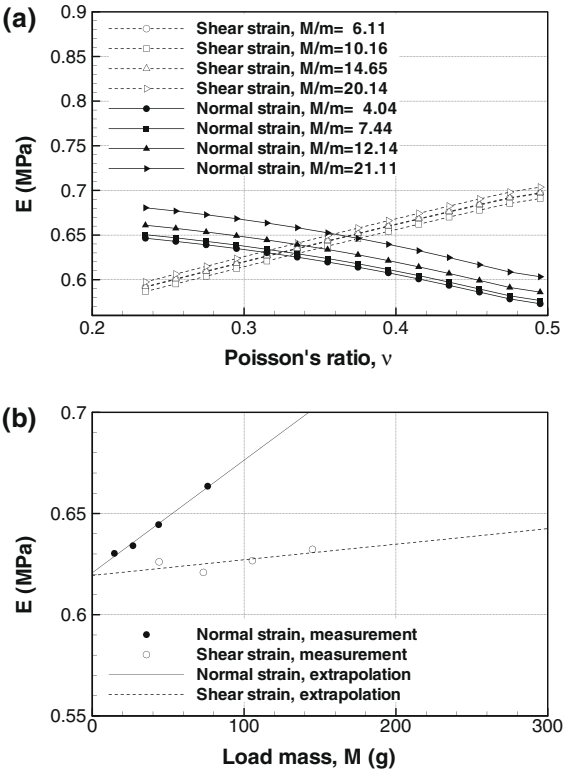

Fig. 7. Initial data at f = 171.9 Hz; (a) variation of Poisson's ratio and (b) variation of load mass.

region of ν. In an ideal case they should intersect at a point, of which abscissa indicates the Poisson's ratio of the material. However, both shear and stress measurements obtained at different load masses are shifted to each other in a systematic manner. The intersection point moves to smaller values of ν for smaller mass ratio M/m. The possible reason for this effect is illustrated in Fig. 8. It consists in the barreling of cylindrical samples under the effect of static loading (dash lines) which leads to decrease of the sample height as $\Delta H = H_0(1-gM/SE)$. However, it was found that the height change compensation in calculating the viscoelastic properties did not provide substantial improvement in the behavior of the curves. Proper direct account for the static barreling requires modification of Eqs. (7) and (8) (respectively, Eqs. (15) and (16)), which makes the calculations more complicated. Hence, we decided to perform the measurements with varying load masses and then linearly extrapolate them to $M = 0$, as shown in Fig. 7(b). Solid line in Fig. 8 sketches a curved side surface of a sample, which is a consequence of addition of the static and dynamic deformations. Conditions of Eqs. (7) and (8) should be satisfied at this surface. Since the application of those conditions in such a way is extremely difficult, we propose a technique of extrapolation of the results to zero load mass.

It is worthwhile to mention that in all tests for the same material the curves $E(M)$ cross about $M = 0$, indicating the reliability of the present procedure. The final values of E were taken as mean values of the extrapolated shear and stress values at $M = 0$. The linear extrapolation of the results at $M = 0$ made it possible to substantially improve the accuracy of determination of the viscoelastic parameters. The accuracy of the method is enhanced also, as the dynamic deformation of the sample is reduced. For each particular material at a fixed frequency the viscoelastic parameters are determined by the intersection of effective curves obtained on calculating the shear and axial deformations at zero load mass. This corresponds to the leftmost intersection point (see Fig. 7(a)).

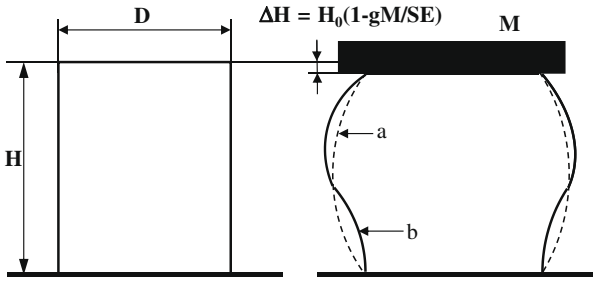

Fig. 8. Deformation of cylindrical specimen under the effect of static and dynamic loading.

As mentioned above, the viscoelastic properties can be obtained from the measurement data for one pair of cylindrical and annular samples. Fig. 9 illustrates an important feature regarding the effect of geometrical sizes of the samples on the calculated viscoelastic properties. Results of measuring three pairs of the samples are shown. The sample #1, which consisted of four cylinders (D10 × H10) was selected for the axial stress measurement. The three pairs are formed by combining the sample #1 and each of three annular samples (#4, #5 and #6), respectively. The first sample for the shear measurements (sample #4) had radial "width" $(D_{out} - D_{in})/2$ =3.5 mm and height 16.95 mm, giving the height to width ratio of 4.84. The second sample (sample #5) had approximately twice larger linear dimensions with the ratio being 4.0. On the contrary, the radial size of the third sample (sample #6) was close to the first sample with the height to width ratio being only 2.0.

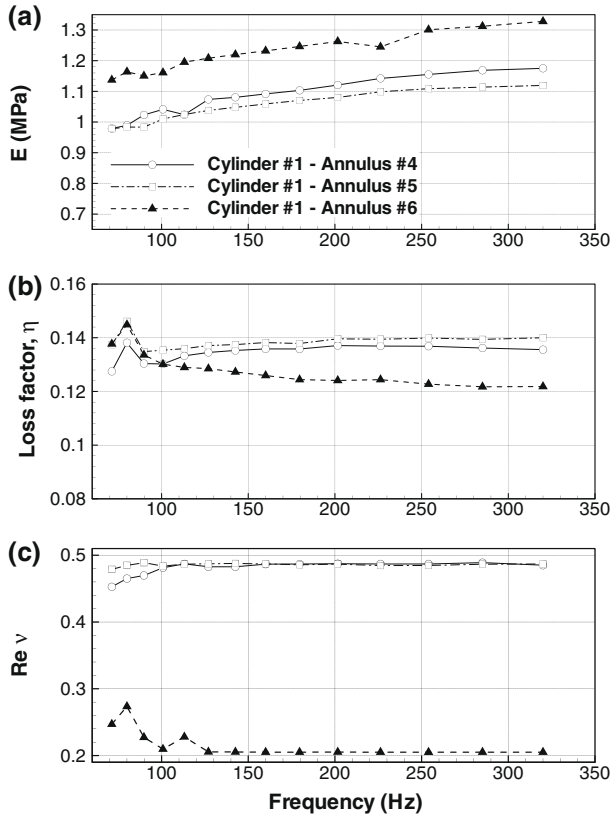

Fig. 9. Calculated viscoelastic properties; (a) modulus of elasticity E, (b) loss factor μ and (c) Poisson's ratio ν.

Modules of elasticity (Fig. 9(a)) and loss factors (Fig. 9(b)) of the first pair (designated as "Cylinder #1–Anulus #4") and the second pair ("Cylinder #1–Anulus #5") are quite close to each other. However, the third pair ("Cylinder #1–Anulus #6") shows quite a large difference from others. Most notable difference is the change of the calculated Poisson's ratio in Fig. 9(c). The same phenomena were observed in all six other pairs of samples studied, where Cylinder #2 (D30 × H30) and Cylinder #3 (D40 × H40) were used for the stress measurements (not shown here for brevity). This can be explained by some edge effects, which manifest themselves when the height of the samples for shear measurements is shortened.

As mentioned above, the determination of the Poisson's ratio is the major goal of the present study. Viscoelastic properties for three pairs of samples, where a large-size annular sample (#5) was fixed for shear measurements in Fig. 10. In the frequency range from 50 to 320 Hz, the calculated modules of elasticity (Fig. 10(a)), the loss factor (Fig. 10(b)) and the real part of the Poisson's ratio (Fig. 10(c)) are virtually unchanged, as the geometrical sizes experience 4 times variations. Tests with varying values of the imaginary part of the Poisson's ratio from −0.1 to 0.1 did not cause any significant change in E. Similarly, the variations of real part of the Poisson's ratio did not affect the loss factor. Hence, after the estimation of E and real part of the Poisson's ratio, the loss factor was estimated in a similar manner as before with varying the imaginary part of the Poisson's ratio.

The imaginary part of the Poisson's ratio in Fig. 10(d) is of particular interest. The curves for different sample sizes diverge at high frequencies. At small frequencies (60–150 Hz), they are on the contrary almost constant and quite close to each other, being about 0.04–0.06. Similar result was obtained at small frequencies for the other three pairs of samples, when sample No. 4 was used for the shear measurements.

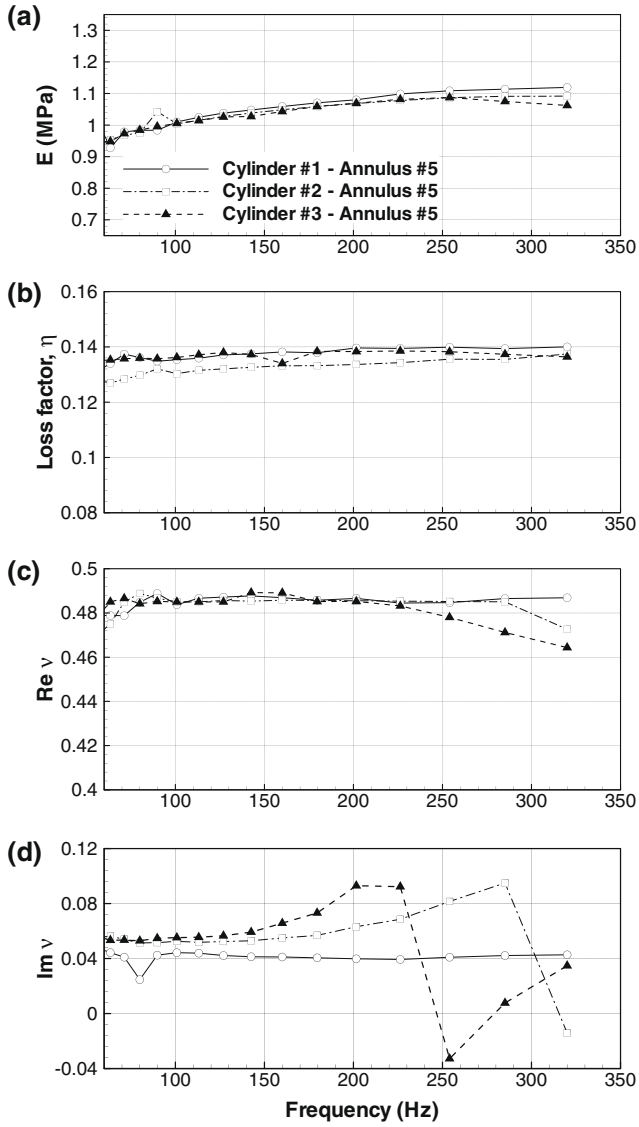

Fig. 10. Calculated viscoelastic properties; (a) modulus of elasticity$E$, (b) loss factorμ, (c) real part of Poisson's ratio and (d) imaginary part of Poisson's ratio.

4. Conclusions

The method of determination of the viscoelastic properties of the materials by means of measuring the forced vibration response of the cylindrical and the annular samples is suggested. A technique to calculate the dynamic modulus of elasticity, loss factor and dynamic complex-number Poisson's ratio based on a two-dimensional model of the sample deformation was proposed. The viscoelastic properties of silicone RTV rubber Silastic S2 were determined. The samples for axial strain and shear strain measurements were manufactured simultaneously of the same mixture. The measurements were performed at small amplitudes in the linear region of the dynamic deformations at temperature 25 °C. With a view to enhancing the calculation accuracy of the viscoelastic properties, a technique of extrapolation of the results of the measurements to zero load mass was proposed. As the geometric sizes of the axial stress samples vary four times, the viscoelastic properties are virtually unchanged. The role of the edge effects becomes substantial as height to width ratio of a sample is reduced from 4 to 2. In the frequency range from 50 to 320 Hz the measured real part of the Poisson's ratio appeared

to be about 0.48, while the imaginary one being 0.04–0.06 at least at small frequencies.

Acknowledgments

This work was financially supported by Russian Foundation for Basic Research No 06-08-00193-a and the ERC program (Advanced Ship Engineering Research Center) of MOST/KOSEF.

References

Canuto, C., Hussaini, M.Y., Quarterony, A., Zang, T.A., 1988. Spectral Methods in Fluid Dynamics, Springer Series in Computational Physics. Springer, Berlin.

Clifton, R.J., Jia, X., Jiao, T., Bull, C., Haln, M.S., 2006. Viscoelastic response of vocal fold tissues and scaffolds and high frequencies. In: Holzapfel, G.A., Ogden, R.W. (Eds.), Mechanics of Biological Tissue. Springer, pp. 445–455.

Crowson, R.J., Arridge, R.G.C., 1979. Linear viscoelastic properties of epoxy resin polymers in dilatation and shear in the glass transition region. 1. Time–temperature superposition of creep data. Polymer 20, 737–746.

Ferry, J.D., 1961. Viscoelastic Properties of Polymers, New York–London.

Giovagnoni, M., 1994. On the direct measurement of the dynamic Poisson's ratio. Mechanics of Materials 17, 33–46.

Grinchenko, V.T., Meleshko, G.L., 1981. Harmonic oscillations and waves in elastic bodies, Kiev, Naukova dumka, p. 284 (in Russian).

Hausler, K.G., Hauptmann, P., Meischner, C., Fedtke, M., Hartel, E., Wartewig, S., 1987. Ultrasonic investigations of modified epoxies. Polymer Communications 28, 154–157.

Kästner, S., Pohl, G., 1963. Ein Beitrag zur Frage der Voltständigen Erfassung des mechanischen Relaxationsverhaltens der Polymeren. Colloid and Polymer Science 191 (2), 114–123.

Koppelmann, V.J., 1959. Uber den dynamischen Elastizitätsmodul von Polymethacrylsäuremethylester bei sehr tiefen Frequenzen. Colloid and Polymer Science 164 (1), 31–34.

Kulik, V.M., Semenov, B.N., 1986. The two-parametric method for measurements of viscoelastic properties of polymer materials. Metrologiya 4, 32–38.

Kulik, V.M., Semenov, B.N., Boiko, A.V., Seoudi, B.M., Chun, H.H., Lee, I. 2008. Measurement of Dynamic Properties of Viscoelastic Materials, Experimental Mechanics. doi:10.1007/s11340-008-9165-x.

Lakes, R.S., Wineman, A., 2006. On Poisson's ratio in linearly viscoelastic solids. Journal of Elasticity 85, 45–63.

Landau, L.D., Lifschitz, E.M., 1986. Theory of Elasticity, third ed. Pergamon Press, Oxford, England.

Riande, E., Diaz-Calleja, R., Prolongo, M.G., Masegosa, R.M., Salom, C., 2000. Polymer viscoelasticity. Stress and Strain in Practice. Marcel Dekker Inc., New York, Basel.

Tang, T., Trummer, M.R., 1996. Boundary layer resolving pseudospectral methods for singular perturbation problems. SIAM Journal on Scientific Computing 17 (2), 430–438.

Timoshenko, S.P., 1953. History of strength of materials. With a Brief Account of the History of Theory of Elasticity and Theory of Structures. McGraw-Hill, New York.

Trefethen, L.N., 1990. Approximation theory and numerical linear algebra. In: Mason, J., Cox, M. (Eds.), Algorithms for Approximation II. Chapman and Hall, London, pp. 336–361.

Tschoegl, N.W., Knauss, W.G., Ermi, I., 2002. Poisson's ratio in linear viscoelasticity – a critical review. Mechanics of Time-Dependent Materials 6, 3–51.

Willis, R.L., Wu, L., Berthelot, Y.H., 2001. Determination of the complex Young and shear dynamic moduli of viscoelastic materials. The Journal of the Acoustical Society of America 109 (2), 611–621.